

A class of symplectic integrators with adaptive timestep for separable Hamiltonian systems

Miguel Preto and Scott Tremaine

Princeton University Observatory, Peyton Hall, Princeton, NJ 08544, USA

ABSTRACT

Symplectic integration algorithms are well-suited for long-term integrations of Hamiltonian systems because they preserve the geometric structure of the Hamiltonian flow. However, this desirable property is generally lost when adaptive timestep control is added to a symplectic integrator. We describe an adaptive-timestep symplectic integrator that can be used if the Hamiltonian is the sum of kinetic and potential energy components and the required timestep depends only on the potential energy (e.g. test-particle integrations in fixed potentials). In particular, we describe an explicit, reversible, symplectic, leapfrog integrator for a test particle in a near-Keplerian potential; this integrator has timestep proportional to distance from the attracting mass and has the remarkable property of integrating orbits in an inverse-square force field with only “along-track” errors; i.e. the phase-space shape of a Keplerian orbit is reproduced exactly, but the orbital period is in error by $O(N^{-2})$, where N is the number of steps per period.

1. Introduction

During the last decade a great deal of effort has been devoted to the development of symplectic integration algorithms (SIAs) for Hamiltonian systems (Channell & Scovel 1990, Yoshida 1993, Marsden, Patrick & Shadwick 1996). An SIA is a symplectic mapping of phase space $\mathbf{z} = (\mathbf{q}, \mathbf{p})$ and time, $\mathbf{M}_h : (\mathbf{z}, t) \rightarrow (\mathbf{z}', t' = t + h)$, that approximates the Hamiltonian flow over a small interval h . SIAs preserve much of the geometric structure of the Hamiltonian flow; as a result, they usually have only oscillatory and not secular errors in the integrals of motion and are useful when the main goal is minimizing long-term qualitative errors rather than achieving the highest possible short-term precision.

The most popular SIA is the leapfrog or Verlet method, which can be applied to separable Hamiltonians of the form

$$H(\mathbf{q}, \mathbf{p}, t) = T(\mathbf{p}) + U(\mathbf{q}, t) \quad (1)$$

(usually T and U are the kinetic and potential energy). We may define “drift” and “kick” operators

$$\mathbf{D}_h : (\mathbf{q}, \mathbf{p}, t) \rightarrow \left(\mathbf{q} + h \frac{\partial T}{\partial \mathbf{p}}, \mathbf{p}, t + h \right), \quad \mathbf{K}_h : (\mathbf{q}, \mathbf{p}, t) \rightarrow \left(\mathbf{q}, \mathbf{p} - h \frac{\partial U}{\partial \mathbf{q}}, t \right), \quad (2)$$

and the leapfrog operator is then

$$\mathbf{L}_h = \mathbf{D}_{h/2} \mathbf{K}_h \mathbf{D}_{h/2}, \quad \text{or} \quad \mathbf{L}_h = \mathbf{K}_{h/2} \mathbf{D}_h \mathbf{K}_{h/2}; \quad (3)$$

either of which defines a second-order SIA (“DKD leapfrog” and “KDK” leapfrog). Higher-order SIAs can be derived by concatenating leapfrog operators; for example $\mathbf{L}_{x_1 h} \mathbf{L}_{x_0 h} \mathbf{L}_{x_1 h}$ is a fourth-order SIA if $x_0 = -2^{1/3}/(2 - 2^{1/3})$, $x_1 = 1/(2 - 2^{1/3})$ (Yoshida 1990). Leapfrog and its higher-order generalizations have several appealing features: only a small number of force evaluations is required per step (1 for a second-order integrator, 3 for a fourth-order integrator); no auxiliary variables are required, thus minimizing memory requirements; and the integrators are explicit and time-reversible.

One limitation of SIAs is that they are usually restricted to a fixed timestep. When a standard adaptive-timestep prescription is applied to an SIA, its performance is no better than that of non-symplectic integrators; the reason is that the mapping $\mathbf{M}_{h(\mathbf{z})}(\mathbf{z}, t)$ is not symplectic even when $\mathbf{M}_h(\mathbf{z}, t)$ is. This is a serious limitation, since in most applications a fixed timestep is inefficient.

There have been many attempts to construct adaptive-timestep SIAs. In the context of molecular dynamics, Skeel & Biesiadecki (1994) split the interaction potential into a short-range component (rapidly varying, cheap to calculate, zero outside a limited range) and a long-range component (slowly varying, expensive to calculate); they then evaluate the effects of the short-range potential every timestep using a symplectic integrator, adding in N times the long-range potential at every N^{th} timestep. This procedure retains symplecticity and can be generalized by splitting the potential into any number of parts. Duncan, Levison & Lee (1998) describe a variant of the Skeel-Biesiadecki method for long-term integrations of solar-system orbits.

In some situations an adaptive-timestep integrator can be replaced by an integrator that uses different—but constant—timesteps for different subsystems. In the context of solar system integrations, Saha & Tremaine (1994) describe an SIA that uses a different timestep for each planet, which works well so long as the planetary orbits are well-separated.

An alternative to adaptive-timestep SIAs is to abandon symplecticity but demand that the integrator is time-reversible. Formally, an integrator is reversible if

$\mathbf{M}_h \mathbf{T} \mathbf{M}_h = \mathbf{T}$ where \mathbf{T} is the time-reversal operator. Reversible maps have many of the same geometric properties as symplectic maps (Arnold 1984 calls the similarities “astonishing”) and hence we expect that reversible integration algorithms have similar virtues to SIAs when they are applied to reversible Hamiltonian systems. In particular we expect that reversible methods should not exhibit secular errors in the integrals of motion.

Reversible integration algorithms with adaptive timestep are relatively easy to generate. Any integration algorithm \mathbf{N}_h can be converted to many reversible algorithms of the same order (Hut et al. 1997); one example is $\mathbf{M}_h \equiv \mathbf{N}_{h/2} \mathbf{T} \mathbf{N}_{h/2}^{-1} \mathbf{T}$. Moreover any reversible integration algorithm remains reversible with variable timestep if the timestep depends symmetrically on the initial and final phase-space coordinates (Hut, Makino & McMillan 1995); unfortunately such integrators are usually implicit and therefore slower than explicit integrators. Various explicit reversible integrators with adaptive timestep are described by Huang & Leimkuhler (1997), Quinn et al. (1997), Calvo et al. (1998), and Evans & Tremaine (1999).

One problem that requires adaptive timestep is the integration of highly eccentric near-Keplerian orbits (e.g. long-period comets, which often have eccentricities $e > 0.99995$). Here the standard approach is to regularize the equations of motion; in particular the Kustaanheimo-Stiefel (KS) regularization converts the Keplerian Hamiltonian to a harmonic oscillator Hamiltonian, which is easier to integrate numerically. KS regularization can be extended to handle few-body problems but is restricted to inverse-square interparticle forces. This technique is also useful in simulations of star clusters, to deal with the delicate problem of the formation and dynamical evolution of tightly-bound binary stars over very long times (e.g. Mikkola & Aarseth 1993). Mikkola (1997, see also Rauch & Holman 1999) has combined KS regularization with an efficient SIA designed for nearly integrable problems by Wisdom & Holman (1991) to provide a sophisticated integrator for eccentric near-Keplerian orbits.

A closely related problem in numerical celestial mechanics is the long-term integration of moderate-eccentricity planet-crossing orbits (e.g. Earth-crossing asteroids, Centaurs, Jupiter-family comets), which are nearly Keplerian for millions of years, yet occasionally suffer strong perturbations from close planetary encounters that may only last a few hours (Duncan et al. 1998).

The aim of this paper is to discuss a class of explicit adaptive-timestep SIAs that can be used to follow Hamiltonian systems of the form (1) in the important special case where the timestep depends only on the potential energy $U(\mathbf{q}, t)$. We provide a brief review of SIAs in §2, and discuss the use of extended phase space

to derive adaptive-timestep SIAs in §3. A class of explicit adaptive-timestep SIAs that are particularly suitable for following orbits in nearly Keplerian potentials is presented in §4, and numerical tests are described in §5. Section 6 contains a brief summary.

As this work neared completion, we learned of a paper by Mikkola & Tanikawa (1999) that contains many similar conclusions.

2. Review of symplectic integration

A SIA is a mapping of the form $\mathbf{M}_h : (\mathbf{z}, t) \rightarrow (\mathbf{z}', t' = t + h)$ where \mathbf{M}_h is symplectic and \mathbf{z}' approximates the phase-space trajectory of \mathbf{z} over time h , which is given by

$$\dot{\mathbf{z}} = \{\mathbf{z}, H\}, \quad (4)$$

where $H(\mathbf{z}, t)$ is the Hamiltonian and the braces stand for the Poisson bracket.

The SIA can be defined implicitly by a generating function $W = W(\mathbf{q}, \mathbf{p}', t)$, with the equations of transformation

$$\mathbf{p} = \frac{\partial W}{\partial \mathbf{q}}, \quad \mathbf{q}' = \frac{\partial W}{\partial \mathbf{p}'}. \quad (5)$$

In the simplest SIA, the generating function is chosen to be

$$W = \mathbf{q} \cdot \mathbf{p}' + hH(\mathbf{q}, \mathbf{p}', t), \quad (6)$$

which implies

$$\begin{aligned} \mathbf{q}' &= \mathbf{q} + h \frac{\partial H(\mathbf{q}, \mathbf{p}', t)}{\partial \mathbf{p}'}, \\ \mathbf{p}' &= \mathbf{p} - h \frac{\partial H(\mathbf{q}, \mathbf{p}', t)}{\partial \mathbf{q}}. \end{aligned} \quad (7)$$

These equations define an implicit first-order SIA. Higher order schemes can be derived from more complicated generating functions (e.g. Channell & Scovel 1990).

We can go further if the Hamiltonian is separable and autonomous, that is, if

$$H = H_A + H_B \quad (8)$$

where H_A and H_B are time-independent and separately integrable. For a system of this type, the equations of motion can be written as

$$\dot{\mathbf{z}} = \{\mathbf{z}, H_A + H_B\}. \quad (9)$$

We introduce the differential operators $\mathbf{A} = \{\cdot, H_A\}$, $\mathbf{B} = \{\cdot, H_B\}$, and write the formal solution of equation (9) as

$$\mathbf{z}(t) = \exp[t(\mathbf{A} + \mathbf{B})]\mathbf{z}(0). \quad (10)$$

By assumption, we know how to calculate $\exp(t\mathbf{A})$ and $\exp(t\mathbf{B})$. In general, these operators are non-commutative so $\exp[t(\mathbf{A} + \mathbf{B})] \neq \exp(t\mathbf{A})\exp(t\mathbf{B})$. The correct expression is given by the Baker-Campbell-Hausdorff (BCH) identity (Yoshida 1993),

$$\exp(\mathbf{X})\exp(\mathbf{Y}) = \exp(\mathbf{Z}), \quad (11)$$

where $\mathbf{Z} = \mathbf{X} + \mathbf{Y} + \frac{1}{2}[\mathbf{X}, \mathbf{Y}] + \frac{1}{12}[\mathbf{X} - \mathbf{Y}, [\mathbf{X}, \mathbf{Y}]] + \dots$. To construct an explicit symplectic integrator of order n we use the BCH identity to find a set of real numbers (c_i, d_i) such that

$$\exp[h(\mathbf{A} + \mathbf{B})] = \prod_{i=1}^k \exp(c_i h \mathbf{A}) \exp(d_i h \mathbf{B}) + O(h^{n+1}); \quad (12)$$

the integrator is then

$$\mathbf{z}(t = h) = \left[\prod_{i=1}^k \exp(c_i h \mathbf{A}) \exp(d_i h \mathbf{B}) \right] \mathbf{z}(0), \quad (13)$$

where the operators are applied in the order $(c_1, d_1, \dots, c_k, d_k)$; this is an example of the general technique of operator splitting. See Yoshida (1990) for a systematic strategy of finding these numerical coefficients. In the important case of a Hamiltonian of the form (1), this map takes the simple form (cf. eq. 2)

$$\mathbf{q}_{i+1} = \mathbf{q}_i + h c_i \left(\frac{\partial T}{\partial \mathbf{p}} \right)_{\mathbf{p}_i}, \quad \mathbf{p}_{i+1} = \mathbf{p}_i - h d_i \left(\frac{\partial U}{\partial \mathbf{q}} \right)_{\mathbf{q}_{i+1}}, \quad (14)$$

where $\mathbf{z}(0) = \mathbf{z}_1$, $\mathbf{z}(h) = \mathbf{z}_{k+1}$. The usual second-order leapfrog (eq. 3) corresponds to the choice $k = 2$, $c_1 = c_2 = \frac{1}{2}$, $d_1 = 1$ and $d_2 = 0$ for DKD leapfrog (or $c_1 = 0$, $c_2 = 1$, $d_1 = d_2 = \frac{1}{2}$ for KDK leapfrog). Using the BCH identity, one can show that

$$\exp(\frac{1}{2}h\mathbf{A})\exp(h\mathbf{B})\exp(\frac{1}{2}h\mathbf{A}) = \exp[h(\mathbf{A} + \mathbf{B} + \mathbf{C})] \quad \text{where} \quad \mathbf{C} = \{\cdot, H_{\text{err}}\} \quad (15)$$

and

$$H_{\text{err}} = \frac{h^2}{12} \{ \{H_A, H_B\}, H_B + \frac{1}{2}H_A \} + O(h^4). \quad (16)$$

Thus DKD leapfrog describes the equations of motion in a surrogate Hamiltonian

$$\widetilde{H} = H + H_{\text{err}}; \quad (17)$$

(more precisely the numerical trajectory lies exponentially close to the exact trajectory of the surrogate Hamiltonian). The good properties of symplectic integrators, such as the absence of secular errors in the energy, are a consequence of the existence of this Hamiltonian.

3. Variable timestep and extended phase space

We want to construct an explicit adaptive-timestep SIA to integrate the Hamiltonian (1). Following Mikkola (1997), we extend phase space by introducing a fictitious time variable τ through the relation

$$dt = g(\mathbf{q}, \mathbf{p}, t)d\tau \tag{18}$$

and take $t \equiv q_0$ as a new coordinate together with the corresponding conjugate momentum $p_0 = -H$. Thus an extended phase space is defined by

$$\mathbf{Q} = (q_0, \mathbf{q}), \quad \mathbf{P} = (p_0, \mathbf{p}), \tag{19}$$

and the equations of motion in the extended phase space are

$$\begin{aligned} \frac{d\mathbf{Q}}{d\tau} &= g(\mathbf{q}, \mathbf{p}, t) \frac{\partial H}{\partial \mathbf{P}} = \frac{\partial \Gamma}{\partial \mathbf{P}}, \\ \frac{d\mathbf{P}}{d\tau} &= -g(\mathbf{q}, \mathbf{p}, t) \frac{\partial H}{\partial \mathbf{Q}} = -\frac{\partial \Gamma}{\partial \mathbf{Q}}, \end{aligned} \tag{20}$$

where

$$\Gamma(\mathbf{Q}, \mathbf{P}) = g(\mathbf{q}, \mathbf{p}, q_0)[H(\mathbf{q}, \mathbf{p}, q_0) + p_0], \tag{21}$$

and only trajectories on the hypersurface $\Gamma = 0$ in the extended phase space correspond to solutions of the equations of motion in the original phase space. The equations of motion (20) are Hamiltonian in the extended phase space if Γ is chosen as the Hamiltonian. We can now integrate the equations of motion with an SIA having constant fictitious timestep $\Delta\tau$ in the extended phase space, which is equivalent to a variable timestep $\Delta t = g(\mathbf{q}, \mathbf{p}, t)\Delta\tau$ in the reduced phase space.

The Hamiltonian (21) is not generally separable and hence operator-splitting techniques cannot be used to derive explicit SIAs with arbitrary timesteps. Nevertheless, this approach can yield useful SIAs for specific choices of the timestep function $g(\mathbf{q}, \mathbf{p}, t)$.

3.1. A separable Hamiltonian in extended phase space

We choose the timestep function to be

$$g(\mathbf{Q}, \mathbf{P}) = \frac{f(T_e(\mathbf{P})) - f(-U(\mathbf{Q}))}{T_e(\mathbf{P}) + U(\mathbf{Q})}, \quad (22)$$

where $T_e(\mathbf{P}) = T(\mathbf{p}) + p_0$ and $U(\mathbf{Q}) = U(\mathbf{q}, q_0)$. The Hamiltonian (21) becomes

$$\Gamma(\mathbf{Q}, \mathbf{P}) = f(T_e(\mathbf{P})) - f(-U(\mathbf{Q})), \quad (23)$$

which is separable. The equations of motion are

$$\begin{aligned} \frac{dq_i}{d\tau} &= \frac{\partial \Gamma}{\partial p_i} = f'(T(\mathbf{p}) + p_0) \frac{\partial T(\mathbf{p})}{\partial p_i}, \\ \frac{dt}{d\tau} &= \frac{\partial \Gamma}{\partial p_0} = f'(T(\mathbf{p}) + p_0), \\ \frac{dp_i}{d\tau} &= -\frac{\partial \Gamma}{\partial q_i} = -f'(-U(\mathbf{q}, t)) \frac{\partial U(\mathbf{q}, t)}{\partial q_i}, \\ \frac{dp_0}{d\tau} &= -\frac{\partial \Gamma}{\partial q_i} = -f'(-U(\mathbf{q}, t)) \frac{\partial U(\mathbf{q}, t)}{\partial t}. \end{aligned} \quad (24)$$

To choose the function f we recall that $H(\mathbf{q}, \mathbf{p}, q_0) + p_0 = T_e(\mathbf{P}) + U(\mathbf{Q}) = 0$ for the Hamiltonian flow, i.e., $T_e(\mathbf{P}) \simeq -U(\mathbf{Q})$ during the numerical integration. Consequently, $f(T_e) - f(-U) \simeq 0$ and we can Taylor expand the function f around $T_e(\mathbf{P})$ to obtain

$$f(T_e(\mathbf{P})) = f(-U(\mathbf{Q})) + [T_e(\mathbf{P}) + U(\mathbf{Q})]f'(-U(\mathbf{Q})) + \mathcal{O}(T_e + U)^2. \quad (25)$$

Therefore, equation (22) yields

$$g(\mathbf{Q}, \mathbf{P}) \simeq f'(-U) \quad (26)$$

along the integration path. Thus the timestep can be chosen to be an arbitrary function of the potential energy, $g = g(-U)$, and a suitable $f(-U)$ is determined by integrating $g(-U)$.

The choice of the timestep function is crucial to the success of an integrator, and the restriction that this function depends only on the potential energy U is severe. Nevertheless timestep functions of this form can be useful for a variety of dynamical problems.

3.2. Error analysis

We now illustrate how to analyze the integration errors that arise when fixed-timestep SIAs are used to integrate the equations of motion (24) in extended phase space. For simplicity we shall assume that the potential is stationary, $U(\mathbf{Q}) = U(\mathbf{q})$, and restrict our attention to DKD leapfrog.

The error Hamiltonian for DKD leapfrog applied to the Hamiltonian (23) is

$$\begin{aligned} \Gamma_{\text{err}}(\mathbf{Q}, \mathbf{P}) = & \frac{1}{12}(\Delta\tau)^2 [f'(-U)]^2 U_{,i}U_{,j} [f''(T_e)p_i p_j + f'(T_e)\delta_{ij}] \\ & - \frac{1}{24}(\Delta\tau)^2 [f'(T_e)]^2 p_i p_j [-f''(-U)U_{,i}U_{,j} + f'(-U)U_{,ij}] + \text{O}(\Delta\tau)^4, \end{aligned} \quad (27)$$

where $U_{,i} = \partial U / \partial q_i$ and summation over the indices $i, j \in \{1, 2, 3\}$ is assumed.

Once we have the error Hamiltonian, the numerical error in the energy in the original phase space is easy to derive. The integrator accurately follows the trajectory of the surrogate Hamiltonian

$$\tilde{\Gamma} = \Gamma + \Gamma_{\text{err}} = f(T_e) - f(-U) + \Gamma_{\text{err}}; \quad (28)$$

thus $\tilde{\Gamma}$ is conserved along the numerical trajectory. At the starting point $(\mathbf{Q}_i, \mathbf{P}_i)$, $\Gamma = 0$ so $\tilde{\Gamma} = \Gamma_{\text{err}}(\mathbf{Q}_i, \mathbf{P}_i) \equiv \Gamma_i$ throughout the integration. Since $\tilde{\Gamma}$ is independent of the coordinate q_0 , the momentum p_0 is conserved throughout the integration and is therefore equal to minus the initial energy E_i . Thus $T_e = T(\mathbf{p}) + p_0 = \Delta E - U(\mathbf{q})$ where $\Delta E = E - E_i$ is the energy error. Equation (28) can now be rewritten as

$$\Gamma_i = f(\Delta E - U(\mathbf{q})) - f(-U(\mathbf{q})) + \Gamma_{\text{err}}(\mathbf{Q}, \mathbf{P}); \quad (29)$$

since the energy error is small we can expand in a Taylor series to obtain

$$\Delta E = \frac{\Gamma_i - \Gamma_{\text{err}}(\mathbf{Q}, \mathbf{P})}{f'(-U(\mathbf{q}))}. \quad (30)$$

4. Keplerian two-body problem

The long-term integration of nearly Keplerian orbits is central to the study of solar system dynamics, and the Keplerian two-body problem provides a natural laboratory for testing integration algorithms.

For simplicity we work in two dimensions, and to provide more general formulae we add an extra potential $V(\mathbf{q}, t)$ to the point-mass potential that defines the Keplerian problem. The Hamiltonian for a test particle is thus

$$H(\mathbf{q}, \mathbf{p}, t) = \frac{1}{2}\mathbf{p}^2 - \frac{\mu}{r} + V(\mathbf{q}, t), \quad (31)$$

where $\mathbf{q} = (x, y)$, $\mathbf{p} = \mathbf{v} = (v_x, v_y)$, $r^2 = x^2 + y^2$, and μ is the mass. The equations of motion are

$$\frac{d^2x}{dt^2} = \frac{dv_x}{dt} = -\mu \frac{x}{r^3} - \frac{\partial V}{\partial x}, \quad \frac{d^2y}{dt^2} = \frac{dv_y}{dt} = -\mu \frac{y}{r^3} - \frac{\partial V}{\partial y}. \quad (32)$$

There are two natural choices for the timestep function $g(\mathbf{q}, \mathbf{p})$ when integrating bound Keplerian orbits: (i) $g \propto r^{3/2}$ ensures that the timestep is a constant fraction of the local free-fall time $t_{\text{ff}} \sim r^{3/2}\mu^{-1/2}$, so that all phases of highly eccentric orbits are followed with the same relative accuracy; (ii) $g \propto r$ ensures that the coordinate trajectory as a function of the fictitious time is that of a harmonic oscillator, so there are no high-frequency harmonics that are difficult for numerical integrators to follow.

We can accommodate both of these choices by assuming that the timestep function is a power law in radius,

$$g(r) = \epsilon r^\gamma \mu^{1-\gamma}, \quad (33)$$

where ϵ is a constant that parametrizes the size of the timestep; having introduced ϵ we can henceforth set $\Delta\tau = 1$ without loss of generality. Since $U \simeq -\mu/r$ for nearly Keplerian orbits, equation (26) then suggests that we choose

$$f(x) = \begin{cases} \frac{\epsilon\mu}{1-\gamma} x^{-\gamma+1} & \text{if } \gamma \neq 1, \\ \epsilon\mu \log x & \text{if } \gamma = 1. \end{cases} \quad (34)$$

The corresponding Hamiltonian is

$$\Gamma(\mathbf{Q}, \mathbf{P}) = \begin{cases} \frac{\epsilon\mu}{1-\gamma} ([T_e(\mathbf{P})]^{-\gamma+1} - [-U(\mathbf{Q})]^{-\gamma+1}) & \text{if } \gamma \neq 1 \\ \epsilon\mu (\log[T_e(\mathbf{P})] - \log[-U(\mathbf{Q})]) & \text{if } \gamma = 1. \end{cases} \quad (35)$$

For the problem we consider here, $U(\mathbf{Q}) = -\mu/(x^2 + y^2)^{1/2} + V(x, y, t)$ and $T_e(\mathbf{P}) = \frac{1}{2}(v_x^2 + v_y^2) + p_0$. The equations of motion (24) in the fictitious time read

$$\begin{aligned} \frac{dx}{d\tau} &= \epsilon\mu \frac{v_x}{(\frac{1}{2}v_x^2 + \frac{1}{2}v_y^2 + p_0)^\gamma} \\ \frac{dy}{d\tau} &= \epsilon\mu \frac{v_y}{(\frac{1}{2}v_x^2 + \frac{1}{2}v_y^2 + p_0)^\gamma} \\ \frac{dt}{d\tau} &= \epsilon\mu \frac{1}{(\frac{1}{2}v_x^2 + \frac{1}{2}v_y^2 + p_0)^\gamma}, \\ \frac{dv_x}{d\tau} &= -\frac{\epsilon\mu}{(\mu/r - V)^\gamma} \left(\frac{\mu x}{r^3} + \frac{\partial V}{\partial x} \right), \end{aligned}$$

$$\begin{aligned}\frac{dv_y}{d\tau} &= -\frac{\epsilon\mu}{(\mu/r - V)^\gamma} \left(\frac{\mu y}{r^3} + \frac{\partial V}{\partial y} \right), \\ \frac{dp_0}{d\tau} &= -\frac{\epsilon\mu}{(\mu/r - V)^\gamma} \frac{\partial V}{\partial t},\end{aligned}\tag{36}$$

These equations can be integrated using leapfrog, since the right-hand sides of the first three depend only on momenta in the extended phase space, and the latter three on coordinates. For example, if the extra potential $V = 0$, then DKD leapfrog for equations (36) with $\gamma = 1$ can be written

$$\begin{aligned}\mathbf{r}_{1/2} &= \mathbf{r} + \frac{\epsilon\mu \mathbf{v}}{v^2 + 2p_0}, \\ t_{1/2} &= t + \frac{\epsilon\mu}{v^2 + 2p_0}, \\ \mathbf{v}' &= \mathbf{v} - \frac{\epsilon\mu \mathbf{r}_{1/2}}{r_{1/2}^2}, \\ \mathbf{r}' &= \mathbf{r}_{1/2} + \frac{\epsilon\mu \mathbf{v}'}{(v')^2 + 2p_0}, \\ t' &= t_{1/2} + \frac{\epsilon\mu}{(v')^2 + 2p_0},\end{aligned}\tag{37}$$

where $r = |\mathbf{r}|$, and p_0 is an integral of motion equal to minus the initial energy. The fictitious time τ is equal to the eccentric anomaly u to within a linear transformation; each step of the integration corresponds to $\Delta u = \epsilon(\mu/a)^{1/2}$ where $a = -\frac{1}{2}\mu/E$ is the semimajor axis.

More generally, if the attracting mass has a trajectory $\mathbf{r}_*(t)$ DKD leapfrog with $\gamma = 1$ reads

$$\begin{aligned}\mathbf{r}_{1/2} &= \mathbf{r} + \frac{\epsilon\mu \mathbf{v}}{v^2 + 2p_0}, \\ t_{1/2} &= t + \frac{\epsilon\mu}{v^2 + 2p_0}, \\ \mathbf{v}' &= \mathbf{v} - \frac{\epsilon\mu[\mathbf{r}_{1/2} - \mathbf{r}_*(t_{1/2})]}{|\mathbf{r}_{1/2} - \mathbf{r}_*(t_{1/2})|^2}, \\ p'_0 &= p_0 + \frac{\epsilon\mu[\mathbf{r}_{1/2} - \mathbf{r}_*(t_{1/2})] \cdot d\mathbf{r}_*(t_{1/2})/dt}{|\mathbf{r}_{1/2} - \mathbf{r}_*(t_{1/2})|^2}, \\ \mathbf{r}' &= \mathbf{r}_{1/2} + \frac{\epsilon\mu \mathbf{v}'}{(v')^2 + 2p'_0}, \\ t' &= t_{1/2} + \frac{\epsilon\mu}{(v')^2 + 2p'_0}.\end{aligned}\tag{38}$$

An appealing feature of equations (38) is that they contain no square roots, which are the most time-consuming operation in integrating Keplerian orbits

by conventional methods; however, square root evaluations do become necessary with this integrator as soon as the non-Keplerian potential $V(\mathbf{r}, t)$ is non-zero.

4.1. Error analysis for the Kepler problem

To analyze the numerical error of DKD leapfrog with $\gamma = \frac{3}{2}$ we take $f(x)$ from equation (34) and set $\Delta\tau = 1$ in equation (27). The leading term of the error Hamiltonian becomes

$$\Gamma_{\text{err}}(\mathbf{Q}, \mathbf{P}) = \frac{\epsilon^3 \mu^3}{24[-U(\mathbf{q})T_e(\mathbf{P})]^3} \times \left\{ 2T_e^{3/2} |\nabla U|^2 - p_i p_j (-U)^{3/2} U_{,ij} - \left[\frac{3}{2} (-U)^{1/2} + 3T_e^{1/2} \right] (\mathbf{p} \cdot \nabla U)^2 \right\}. \quad (39)$$

For the Kepler problem, $U = -\mu/r$ and the error Hamiltonian simplifies to

$$\Gamma_{\text{err}} = \frac{\epsilon^3 \mu^2}{24T_e^3} \left[\frac{2T_e^{3/2}}{r} - \frac{3T_e^{1/2}(\mathbf{v} \cdot \mathbf{r})^2}{r^3} + \frac{3\mu^{1/2}(\mathbf{v} \cdot \mathbf{r})^2}{2r^{7/2}} - \frac{\mu^{1/2}v^2}{r^{3/2}} \right], \quad (40)$$

where $T_e = \frac{1}{2}v^2 + p_0$.

Similarly, for $\gamma = 1$ the leading term of the error Hamiltonian is

$$\Gamma_{\text{err}}(\mathbf{Q}, \mathbf{P}) = \frac{\epsilon^3 \mu^3}{24[-U(\mathbf{q})T_e(\mathbf{P})]^2} \left[2T_e |\nabla U|^2 + p_i p_j U U_{,ij} - 3(\mathbf{p} \cdot \nabla U)^2 \right]; \quad (41)$$

for the Kepler problem, this simplifies to

$$\Gamma_{\text{err}}(\mathbf{Q}, \mathbf{P}) = \frac{\epsilon^3 \mu^3 p_0}{12r^2(\frac{1}{2}v^2 + p_0)^2}. \quad (42)$$

This formula leads to a remarkable conclusion, specific to this potential and integrator. The original phase-space variables (\mathbf{q}, \mathbf{p}) enter Γ_{err} in the same combination that they enter the Hamiltonian Γ ; in other words the surrogate Hamiltonian may be written

$$\tilde{\Gamma}(\mathbf{Q}, \mathbf{P}) = \Gamma(\mathbf{Q}, \mathbf{P}) + \Gamma_{\text{err}}(\mathbf{Q}, \mathbf{P}) = \epsilon\mu \log W(\mathbf{Q}, \mathbf{P}) + \frac{\epsilon^3 \mu p_0}{12W^2(\mathbf{Q}, \mathbf{P})}, \quad (43)$$

where $W(\mathbf{Q}, \mathbf{P}) = r(\frac{1}{2}p^2 + p_0)/\mu$. Thus the equations of motion (4) for $\tilde{\Gamma}$ read

$$\dot{\mathbf{z}} = \{\mathbf{z}, \tilde{\Gamma}\} = \left(\frac{\epsilon\mu}{W} - \frac{\epsilon^3 \mu p_0}{6W^3} \right) \{\mathbf{z}, W\}, \quad \dot{q}_0 = \frac{\epsilon r}{W} - \frac{\epsilon^3 r p_0}{6W^3} + \frac{\epsilon^3 \mu}{12W^2}, \quad p_0 = \text{const}; \quad (44)$$

while the equations of motion for Γ read

$$\dot{\mathbf{z}} = \{\mathbf{z}, \Gamma\} = \frac{\epsilon\mu}{W}\{\mathbf{z}, W\}, \quad \dot{q}_0 = \frac{\epsilon r}{W}, \quad p_0 = \text{const.} \quad (45)$$

Thus the exact trajectory $\mathbf{z}(\tau)$ (Hamiltonian Γ) is the same as the numerical trajectory $\mathbf{z}(\tau')$ (Hamiltonian $\tilde{\Gamma}$) at a slightly different fictitious time, where the two timescales are related by $d\tau = d\tau'[1 - \epsilon^2 p_0/(6W^2)]$ or $\tau = \tau'(1 - \epsilon^2 p_0)$ since $W = 1$ on the trajectory. In other words the algorithm (38) follows the Keplerian trajectory *exactly*: the position and velocity are precisely those of the Keplerian orbit, and the only error is in the time of arrival at a given location (i.e. the only error is “along-track”)¹. Although we have only established this result to leading order in the error Hamiltonian, we show in the Appendix that it holds at all orders, i.e. for arbitrarily large timesteps. This result also applies in the more general case where the attracting mass is in uniform motion rather than stationary at the origin (cf. eqs. 38).

We also show in the Appendix that the timing error arising from a step Δu in eccentric anomaly is $\frac{1}{12}(\Delta u)^3/n + O(\Delta u)^5$ where $n = (\mu/a^3)^{1/2}$ is the mean motion and the error is independent of eccentricity. The fractional error in the orbital period is then $\pi^2/3N^2$ where N is the number of steps per period (eq. A12).

4.2. Error analysis for the perturbed Kepler problem

Because DKD leapfrog with $\gamma = 1$ follows a Keplerian trajectory exactly, this method is of particular interest for the perturbed Kepler problem, where the extra potential $V(\mathbf{r}, t)$ in equations (36) is small but non-zero. To investigate the errors in this case, we take the error Hamiltonian (41), set $U = -\mu/r + V$ (for simplicity we assume that V is stationary), and expand to first order in V :

$$\begin{aligned} \Gamma_{\text{err}}(\mathbf{Q}, \mathbf{P}) = & \frac{\epsilon^3 \mu^2}{24(\frac{1}{2}v^2 + p_0)^2} \left[\frac{2\mu p_0}{r^2} + \frac{4p_0 V}{r} + 4(\frac{1}{2}v^2 + p_0) \frac{\mathbf{r} \cdot \nabla V}{r} \right. \\ & \left. - r v_i v_j V_{,ij} + \frac{v^2 V}{r} - \frac{3(\mathbf{v} \cdot \mathbf{r})^2 V}{r^3} - 6 \frac{\mathbf{v} \cdot \mathbf{r}}{r} \mathbf{v} \cdot \nabla V \right]. \end{aligned} \quad (46)$$

When this is evaluated on the trajectory, we have

$$\begin{aligned} \Gamma_{\text{err}}(\mathbf{Q}, \mathbf{P}) = & -\frac{1}{12}\epsilon^3 \mu E + \frac{\epsilon^3}{24} \left[-8ErV + 4\mu \mathbf{r} \cdot \nabla V \right. \\ & \left. - r^3 v_i v_j V_{,ij} + r v^2 V - \frac{3(\mathbf{v} \cdot \mathbf{r})^2 V}{r} - 6r(\mathbf{v} \cdot \mathbf{r}) \mathbf{v} \cdot \nabla V \right]. \end{aligned} \quad (47)$$

¹This result holds only for DKD leapfrog, not KDK leapfrog.

The energy error is then (eq. 30)

$$\Delta E = \frac{\Gamma_i - \Gamma_{\text{err}}(\mathbf{Q}, \mathbf{P})}{\epsilon r}. \quad (48)$$

As $r \rightarrow 0$ we have $v \sim r^{-1/2}$. Thus if $V \sim r^k$ as $r \rightarrow 0$, $\Gamma_{\text{err}} \sim r^k$ as well. Then if $k > 0$, the energy error at close encounters with the attracting mass is

$$\Delta E = \frac{\Gamma_i}{\epsilon r}, \quad r \ll r_i; \quad (49)$$

in other words the energy error at close encounters is determined by the initial conditions and varies as r^{-1} , independent of the form of the perturbing potential at small radii so long as $V \rightarrow 0$ as $r \rightarrow 0$.

The divergence of ΔE as $r \rightarrow 0$, even when the perturbing potential $V \rightarrow 0$ as $r \rightarrow 0$, appears to contradict our proof that the integrator tracks Keplerian orbits exactly; the resolution is that the integrator only tracks Keplerian orbits on the hypersurface $\Gamma = 0$ in the extended phase space, and numerical errors at larger radii perturb the trajectory to the neighboring hypersurface $\Gamma = \Gamma_i$. In fact it can be shown that in this case the integrator *is* following a Kepler orbit exactly, but for an attracting mass $\mu \exp(\Gamma_i/\epsilon\mu)$. Thus even large energy errors at close encounters do not signal a catastrophic failure of the integrator, so long as $|\Gamma_i/\epsilon\mu| \ll 1$.

Moreover there is a simple way to correct these errors. Normally the initial value of p_0 is set equal to $-E$, so that $\Gamma = 0$; instead, we modify the initial value of p_0 so that $\tilde{\Gamma} = \Gamma + \Gamma_{\text{err}}$ is zero. This requires

$$p_0 = -E + \frac{\mu}{r} [\exp(-\Gamma_i/\epsilon\mu) - 1]. \quad (50)$$

5. Numerical tests

5.1. Keplerian two-body problem

We have tested these integration methods by following Keplerian orbits with eccentricities $e = 0.9, 0.99, 0.999, 0.9999, 0.99999, \text{ and } 0.999999$. Each orbit is started at pericenter and followed for 2×10^4 orbital periods (although a shorter integration would have been sufficient, since the energy errors are oscillatory rather than growing). We characterize the performance of the integrator by the maximum energy error $|\Delta E_{\text{max}}/E_0| \equiv \max |(E - E_0)/E_0|$, as a function of the number of steps per orbital period.

Figure 1 shows the energy error that arises from integrating equations (36) using DKD leapfrog with $\gamma = \frac{3}{2}$ (i.e. timestep $\propto r^{3/2}$). For comparison we

have also shown as open circles the energy error for leapfrog with fixed timestep ($\gamma = 0$) at eccentricity $e = 0.9$ and 0.99 . Clearly $\gamma = \frac{3}{2}$ provides far more accurate integrations than $\gamma = 0$.

We can compare these energy errors to the analysis of §4.1. When evaluated on the trajectory ($T_e = -U$) the error Hamiltonian (40) is

$$\Gamma_{\text{err}} = -\frac{\epsilon^3 r^{3/2}}{24\mu^{1/2}} \left[\frac{3(\mathbf{r} \cdot \mathbf{v})^2}{2r^2} + 2E \right] = \frac{\epsilon^3 n a^2}{24} \left[(1 - e \cos u)^{3/2} - \frac{3e^2 \sin^2 u}{2(1 - e \cos u)^{1/2}} \right], \quad (51)$$

where as usual n , a , and u are the mean motion, semimajor axis, and eccentric anomaly. The energy error is then given by equation (30),

$$\Delta E = \frac{\epsilon^2 n^2 a^2}{24} \left[\left(\frac{1 - e \cos u_i}{1 - e \cos u} \right)^{3/2} - \frac{3e^2 \sin^2 u_i}{2(1 - e \cos u_i)^{1/2} (1 - e \cos u)^{3/2}} - 1 + \frac{3e^2 \sin^2 u}{2(1 - e \cos u)^2} \right]. \quad (52)$$

For high-eccentricity orbits started at pericenter ($u_i = 0$), the maximum error $|\Delta E|$ occurs at $u \simeq \cos^{-1} e$, and is given by

$$\left| \frac{\Delta E}{E} \right|_{\text{max}} = \frac{\epsilon^2}{16(1 - e)} + \text{O}[\epsilon^2(1 - e)^0]. \quad (53)$$

For high-eccentricity orbits started at apocenter ($u_i = \pi$), the maximum energy error occurs at pericenter,

$$\left| \frac{\Delta E}{E} \right|_{\text{max}} = \frac{\epsilon^2}{3 \cdot 2^{1/2} (1 - e)^{3/2}} + \text{O} \left(\frac{\epsilon^2}{1 - e} \right). \quad (54)$$

These formulae show that pericenter starts lead to smaller energy errors than apocenter starts, although in the latter case the errors can be reduced by the use of corrected initial conditions (cf. §4.2).

The number of steps per orbit $N \simeq \int_0^P dt/g(r)$, where $g(r)$ is the timestep function (33) and P is the orbital period. For $\gamma = \frac{3}{2}$

$$N = \frac{2}{\epsilon} \int_0^\pi \frac{df}{(1 + e \cos f)^{1/2}} = \frac{4}{\epsilon(1 + e)^{1/2}} K \left(\frac{2e}{1 + e} \right), \quad (55)$$

where f is the true anomaly and K is an elliptic integral. Plotting equations (53) and (55) as a parametric function of ϵ we obtain the dashed lines in Figure 1, which agree well with the energy errors from the numerical orbit integrations.

As we discussed in the previous section, integrating the Keplerian equations of motion using DKD leapfrog with $\gamma = 1$ (eq. 37) yields even better behavior than

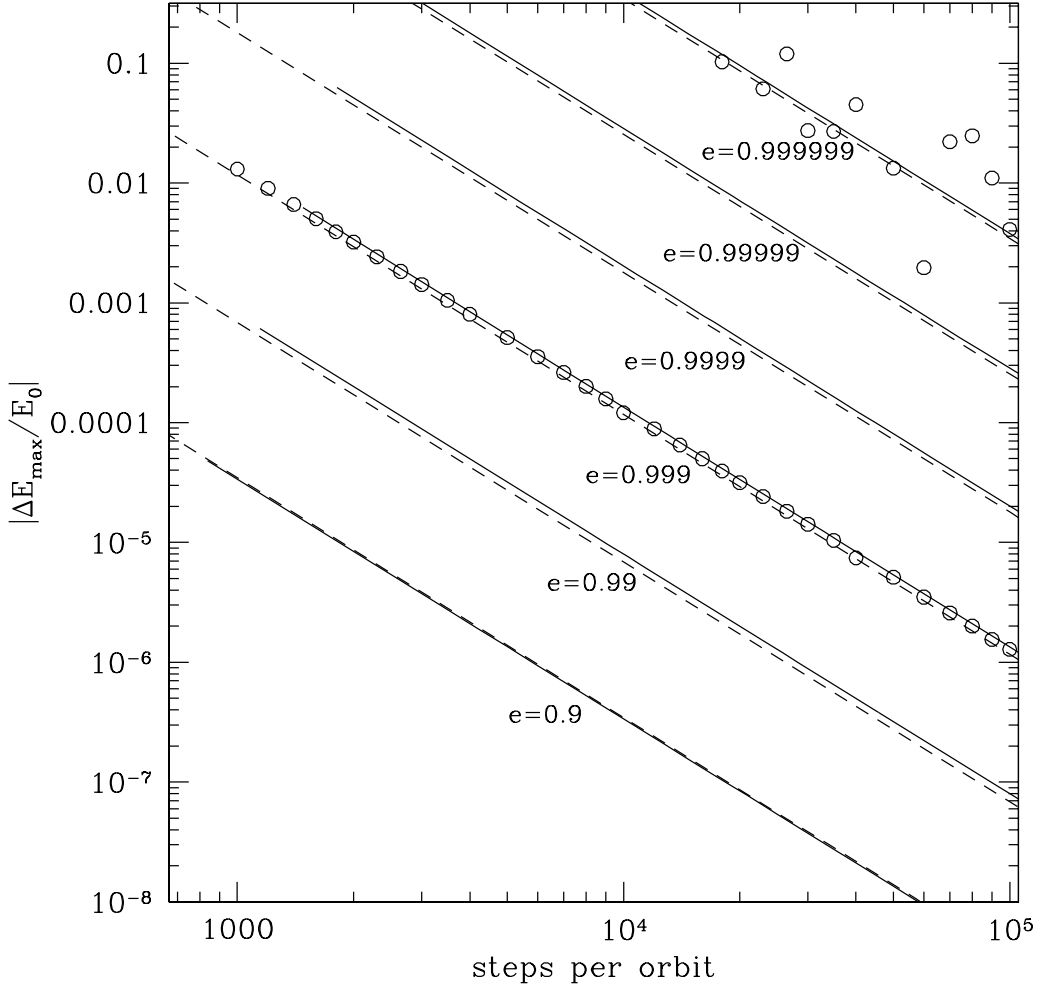


Fig. 1.— Maximum fractional energy error over 2×10^4 orbital periods, as a function of number of steps per orbit for the Keplerian two-body problem. The curves correspond to eccentricities $e = 0.9, 0.99, 0.999, 0.9999, 0.99999, 0.999999$. The integrator is standard DKD (drift-kick-drift) leapfrog with timestep $\propto r^{3/2}$, following equations (33) and (36) with $\gamma = \frac{3}{2}$. The orbits are started at pericenter. The dashed lines show analytic estimates of the energy error from equations (53) and (55). The analogous errors for DKD leapfrog with fixed timestep and $e = 0.9$ and 0.99 are shown as open circles; for larger eccentricities the fixed-timestep errors are off-scale.

$\gamma = \frac{3}{2}$, as in this case the energy error is zero—in fact there is zero error in all of the phase-space functions that are constants of motion in a point-mass potential (energy, angular momentum and Runge-Lenz vector). To test the practical value of this algorithm we must therefore turn to more general Hamiltonians, which we now do.

5.2. The Stark problem

The Stark problem is to follow the motion of a test particle subject to an inverse-square force plus a constant force; the Stark Hamiltonian is

$$H = \frac{1}{2}\mathbf{p}^2 - \frac{\mu}{r} - \mathbf{S} \cdot \mathbf{r}, \quad (56)$$

where the Stark vector \mathbf{S} is a constant. The Stark Hamiltonian has three constants of motion and thus is integrable: these are the energy E , the angular momentum component along \mathbf{S} , and a third analytic integral that we see no point in writing out (Pars 1965, Landau & Lifshitz 1976). We restrict ourselves to the planar case, which is particularly challenging because all orbits oscillate between retrograde and prograde and hence pass arbitrarily close to the attracting mass. We shall examine only a single integrator, DKD leapfrog, applied to the equations of motion for $\gamma = 1$ (eqs. 36), since in this case the trajectory is followed exactly when $\mathbf{S} = 0$.

Rauch & Holman (1999) have recently tested several integrators on the Stark problem, and we shall usually use their initial conditions: the initial eccentricity $e = 0.9$, the Stark vector is oriented 45° to the initial line of apsides, and the orbit is started at apocenter. The strength of the Stark perturbation is written $S = \eta E^2/\mu$ where E is the energy and $\eta \ll 1$ for nearly Keplerian motion.

The error Hamiltonian and the expected energy error are given by equations (47) and (48) with $V = -\mathbf{S} \cdot \mathbf{r}$. Figure 2 verifies the functional form $\Delta E \propto r^{-1}$ predicted by (48) and demonstrates the improvement during close encounters that results from using the corrected initial condition (50).

Figure 3 shows the energy error as a function of steps per orbit N and strength of the Stark parameter, for integrations lasting $n = 10^4$ orbital periods using the Rauch-Holman initial conditions corrected by equation (50). We have plotted both the maximum energy error, which is dominated by very close encounters, and the average of the absolute value of the energy error, which provides a better estimate of the typical error. The average error exhibits the N^{-2} dependence expected for a second-order integrator; the maximum error is much larger and more irregular, reflecting its dependence on rare and rather unphysical close

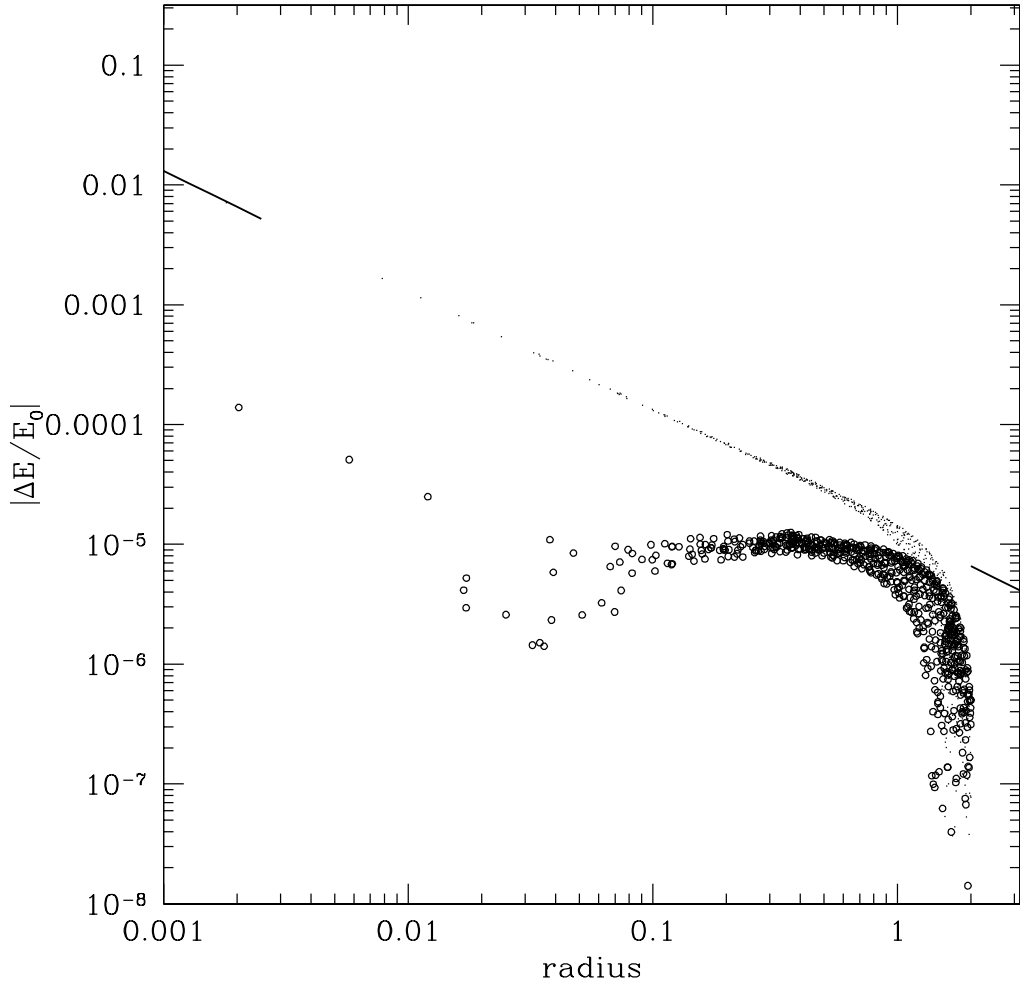


Fig. 2.— Fractional energy error as a function of distance from the attracting mass, for a numerical integration of the Stark problem using DKD leapfrog with $\gamma = 1$, which integrates Keplerian orbits with zero energy error. The integration lasts for 1000 Keplerian periods of the initial orbit and the error is plotted every 100 timesteps. The integration parameters are $\mu = 1$, $\epsilon = 0.1$, the initial eccentricity is $e = 0.9$, the Stark vector is 45° from the initial line of apsides, and its magnitude is $S = \eta E^2/\mu$ where $\eta = 4 \times 10^{-3}$. For $r \ll 1$ the points lie on a straight line, consistent with the prediction of equation (49) marked by solid line segments. The open circles show the much smaller energy errors when the initial conditions are corrected using equation (50).

encounters (the typical maximum eccentricity in an integration of this length is given by $1 - e_{\max} \sim n^{-2} = 10^{-8}$). We have also plotted one error curve for uncorrected initial conditions; we see that the correction reduces the errors by about one order of magnitude in this case.

Rauch & Holman (1999) tested the Wisdom & Holman (1991) integrator on the Stark problem with $\eta = 4 \times 10^{-3}$. They found that the Wisdom-Holman integrator—which works very well for low-eccentricity orbits—was generally unstable, in that the energy error grew by a random walk until the orbit escaped to infinity. The instability arose through numerical chaos caused by the overlap of resonances in the error Hamiltonian, and could only be evaded if the (constant) timestep was in resonance with the orbital period, or is small enough that the pericenter passage is well-resolved—even though the Wisdom-Holman integrator follows Keplerian orbits exactly for any timestep. Our integrator is evidently not subject to these limitations.

Rauch & Holman also tested several other methods. In particular, Mikkola’s regularized version of the Wisdom-Holman mapping was completely stable, and gave energy errors comparable to those shown for our integrator in Figure 3. However, we expect that our method is faster in practice because it requires fewer calculations per integration step.

6. Summary

We have constructed adaptive-timestep, reversible, explicit SIAs for separable Hamiltonians of the form (1), using extended phase space (Mikkola 1997); the principal restriction is that the timestep must be a function of the potential energy alone.

Integrators of this kind would require modifications for problems with many degrees of freedom since the total potential energy of the system is insensitive to local conditions that may demand a short timestep (e.g. a close encounter between two bodies). However, for test-particle integrations in fixed, smooth potentials or few-body systems with similar masses, these integrators can provide both adaptive timestep control and the excellent long-term error control associated with symplectic and reversible integration algorithms.

For close encounters or eccentric orbits in few-body gravitating systems, these adaptive-timestep SIAs provide an attractive alternative to fixed-timestep SIAs in regularized coordinates; moreover, unlike regularized integrators, adaptive-timestep SIAs can also be used to follow orbits in non-Keplerian potentials (e.g. galaxies).

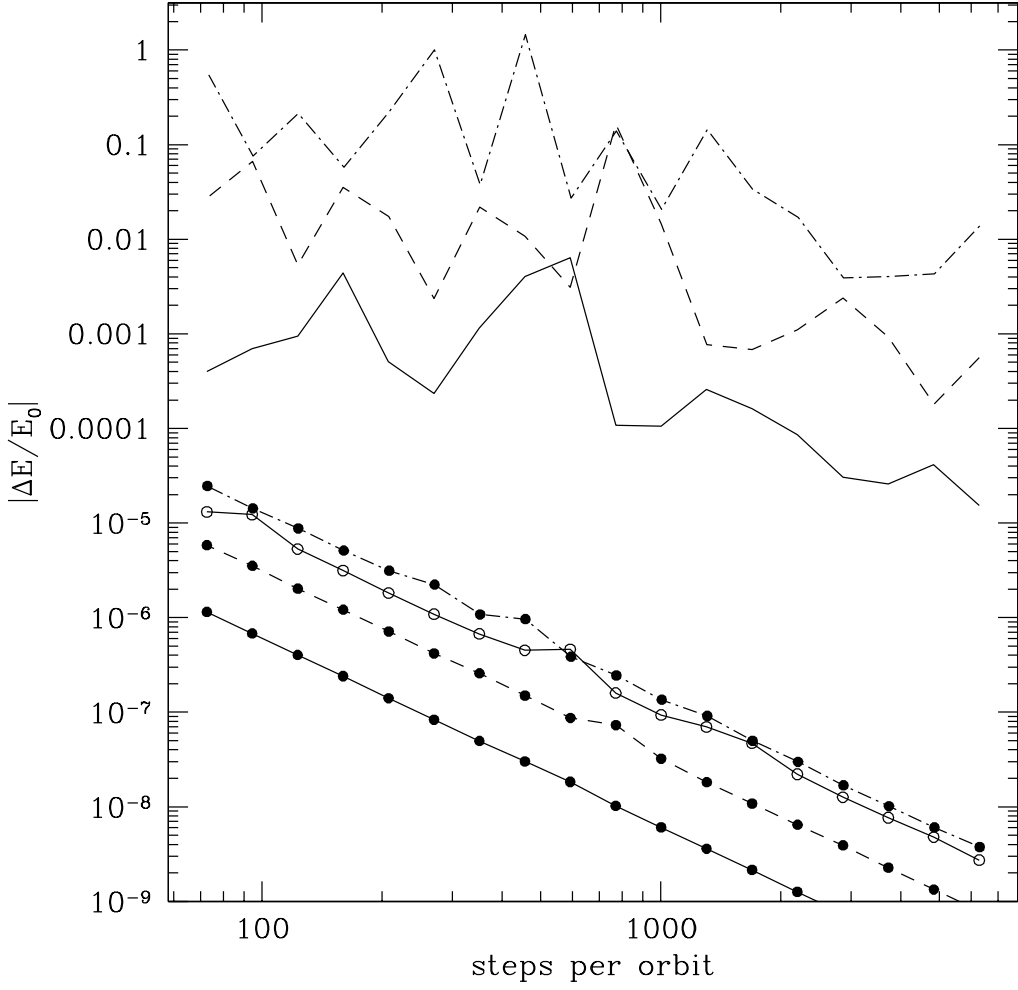


Fig. 3.— Fractional energy error for the Stark problem, as a function of number of force evaluations per orbit. The initial eccentricity is $e = 0.9$, the Stark vector is 45° from the initial line of apsides, and the orbit starts at apocenter and is followed for 10^4 periods. The magnitude of the Stark vector is $S = \eta E^2 / \mu$ where $\eta = 0.001$ (solid lines), 0.005 (dashed lines), and 0.02 (dash-dot lines). The lower curves (solid circles) represent the average of the absolute value of the energy error, and the upper curves the maximum error. The integrator is DKD leapfrog with $\gamma = 1$ and initial conditions corrected using equation (50); the single solid curve with open circles represents the average error for $\eta = 0.001$ if no corrector is applied.

Although we have discussed only second-order leapfrog integrators, higher-order adaptive-timestep SIAs can be derived by concatenating leapfrog steps of different lengths (Yoshida 1990).

A particularly interesting example of these integrators is offered by equations (37), which follow a Keplerian trajectory exactly, with only “along-track” errors.

This research was supported in part by NASA Grant NAG5–7310. We thank Seppo Mikkola for sending us a copy of his paper (Mikkola & Tanikawa 1999), which also shows that the integrator (38) is exact for Keplerian orbits. We also thank Kevin Rauch for thoughtful comments.

A. Appendix: An exact integrator for the Kepler problem

We prove that the $\gamma = 1$ leapfrog integrator (38) follows a Keplerian orbit exactly, except for errors in the time. For simplicity we shall assume that the attracting mass is at rest at the origin, as in equations (37); the extension to an attracting mass in uniform motion is straightforward.

Let (\mathbf{r}, \mathbf{v}) and $(\mathbf{r}', \mathbf{v}')$ be the position and velocity at two points on a bound Keplerian orbit with eccentric anomalies u and u' respectively. Then $(\mathbf{r}', \mathbf{v}')$ satisfies the relation

$$\begin{aligned}\mathbf{r}' &= f(u, u')\mathbf{r} + g(u, u')\mathbf{v} \\ \mathbf{v}' &= f_t(u, u')\mathbf{r} + g_t(u, u')\mathbf{v},\end{aligned}\tag{A1}$$

where

$$\begin{aligned}f(u, u') &= \frac{\cos(u' - u) - e \cos u}{1 - e \cos u}, \\ g(u, u') &= \frac{1}{n} [\sin(u' - u) - e \sin u' + e \sin u], \\ f_t(u, u') &= -\frac{n \sin(u' - u)}{(1 - e \cos u')(1 - e \cos u)}, \\ g_t(u, u') &= \frac{\cos(u' - u) - e \cos u'}{1 - e \cos u'}\end{aligned}\tag{A2}$$

are Gauss's f and g functions (e.g. Danby 1988); here e is the eccentricity, $n = (\mu/a^3)^{1/2}$ is the mean motion and a is the semimajor axis, which is related to the radius through $r = a(1 - e \cos u)$.

These equations can be rewritten as

$$\begin{aligned}\mathbf{r}_{1/2} &= \mathbf{r} + s(u', u)\mathbf{v}, \\ \mathbf{v}' &= \mathbf{v} + z(u', u)\mathbf{r}_{1/2}, \\ \mathbf{r}' &= \mathbf{r}_{1/2} - s(u, u')\mathbf{v}',\end{aligned}\tag{A3}$$

where

$$\begin{aligned}s(u', u) &= \frac{[1 - \cos(u' - u)](1 - e \cos u)}{n \sin(u' - u)}, \\ z(u', u) &= -\frac{n \sin(u' - u)}{(1 - e \cos u')(1 - e \cos u)}.\end{aligned}\tag{A4}$$

Comparison to the $\gamma = 1$ leapfrog integrator (38) shows that the two maps $(\mathbf{r}, \mathbf{v}) \rightarrow (\mathbf{r}', \mathbf{v}')$ are the same if

$$\begin{aligned} \frac{\epsilon\mu}{p^2 + 2p_0} &= \frac{[1 - \cos(u' - u)](1 - e \cos u)}{n \sin(u' - u)}, \\ \frac{\epsilon\mu}{q_{1/2}^2} &= \frac{n \sin(u' - u)}{(1 - e' \cos u')(1 - e \cos u)}, \\ \frac{\epsilon\mu}{(p')^2 + 2p_0} &= \frac{[1 - \cos(u' - u)](1 - e \cos u')}{n \sin(u' - u)}. \end{aligned} \quad (\text{A5})$$

We use the relations $p^2 + 2p_0 = 2\mu/[a(1 - e \cos u)]$, $(p')^2 + 2p_0 = 2\mu/[a(1 - e \cos u')]$ and square the first of equations (A3) to eliminate $q_{1/2}^2$. After some algebra we find that all of the relations (A5) are satisfied if

$$\epsilon = 2 \frac{1 - \cos \Delta u}{na \sin \Delta u}. \quad (\text{A6})$$

where $\Delta u \equiv u' - u$. Thus, we have proved that our mapping follows the Keplerian two-body problem exactly in the original phase space. Although our proof is for bound orbits, it is straightforward to show that unbound Keplerian orbits ($a < 0$) are also integrated exactly, with

$$\epsilon = 2 \frac{\cosh \Delta u - 1}{n_u a \sinh \Delta u}; \quad (\text{A7})$$

here $n_u = (-\mu/a^3)^{1/2}$ and $r = -a(e \cosh u - 1)$.

We must still establish the relation between the timestep given by the second and fifth of equations (38) and the actual time Δt_K required to travel from \mathbf{r} to \mathbf{r}' . The timestep is

$$t' = t + \Delta t = t + \epsilon\mu \left(\frac{1}{p^2 + 2p_0} + \frac{1}{(p')^2 + 2p_0} \right) = t + \frac{1}{2}\epsilon a(2 + e \cos u + e \cos u'). \quad (\text{A8})$$

The relation (A6) then implies that

$$\begin{aligned} n\Delta t &= \frac{[1 - \cos(u' - u)](2 - e \cos u - e \cos u')}{\sin(u' - u)} \\ &= 2 \frac{1 - \cos(u' - u)}{\sin(u' - u)} - e \sin u' + e \sin u. \end{aligned} \quad (\text{A9})$$

On the other hand Kepler's equation states that the actual timestep is given by

$$n\Delta t_K = u' - u - e \sin u' + e \sin u. \quad (\text{A10})$$

Thus the time error is given by

$$n(\Delta t - \Delta t_K) = 2 \frac{1 - \cos \Delta u}{\sin \Delta u} - \Delta u = \frac{1}{12}(\Delta u)^3 + \frac{1}{120}(\Delta u)^5 + O(\Delta u)^7, \quad (\text{A11})$$

independent of eccentricity.

If we take $N = 2\pi/\Delta u$ steps per orbit, the timing error per orbit is

$$\frac{\delta t}{P} = \frac{\pi^2}{3N^2} + O(N^{-4}), \quad (\text{A12})$$

independent of eccentricity.

REFERENCES

- Arnold, V. I. 1984, in *Nonlinear and Turbulent Processes in Physics*, 3, ed. R. Z. Sagdeev (Chur: Harwood), 1161
- Calvo, M. P., López-Marcos, M. A., & Sanz-Serna, J. M. 1998, *App. Num. Math.* 28, 1
- Channell, P. J., & Scovel, J. C. 1990, *Nonlinearity* 3, 231
- Danby, J. M. A. 1988, *Fundamentals of Celestial Mechanics* (Willmann-Bell, Richmond)
- Duncan, M. J., Levison, H. F., & Lee, M. H. 1998, *AJ* 116, 2067
- Evans, N. W., & Tremaine, S. 1999, *AJ*, in press
- Huang, W., & Leimkuhler, B. 1997, *SIAM J. Sci. Comput.* 18, 239
- Hut, P., Makino, J., & McMillan, S. 1995, *Astrophys. J.*, 443, L93
- Hut, P., Funato, Y., Kokubo, E., Makino, J., & McMillan, S. 1997, in *Computational Astrophysics: 12th Kingston Meeting on Theoretical Astrophysics*, eds. D. A. Clarke & M. J. West (San Francisco: Astronomical Society of the Pacific), 26
- Landau, L., & Lifshitz, L. 1976, *Mechanics*, third edition (Oxford: Pergamon)
- Marsden, J., Patrick, G., & Shadwick, W. F., eds. 1996, *Integration Algorithms for Classical Mechanics*, Fields Institute Communications, 10, 217
- Mikkola, S. 1997, *Cel. Mech. Dyn. Astr.* 67, 145
- Mikkola, S., & Aarseth, S. J. 1993, *Cel. Mech. Dyn. Astron.* 57, 439
- Mikkola, S., & Tanikawa, K. 1999, submitted to *Cel. Mech. Dyn. Astron.*
- Pars, L. A. 1965, *A Treatise on Analytical Dynamics* (London: Heinemann)

- Quinn, T. R., Katz, N., Stadel J. & Lake G. 1997, astro-ph/9710043, submitted to *Astrophys. J.*
- Rauch, K. P., & Holman, M. 1999, *AJ*, 117, 1087
- Saha, P., & Tremaine, S. 1994, *AJ* 108, 1962
- Skeel, R. D., & Biesiadecki, J. J. 1994, *Ann. Num. Math.* 1, 191
- Wisdom, J., & Holman, M. 1991, *AJ* 102, 1528
- Yoshida, H. 1990, *Phys. Lett. A* 150, 262
- Yoshida, H. 1993, *Celest. Mech. Dyn. Astron.* 56, 27